JOURNAL OF AIRCRAFT
Vol. 45, No. 6, November–December 2008

Insectlike Flapping Wings in the Hover Part 1: Effect of Wing Kinematics

Salman A. Ansari,* Kevin Knowles,† and Rafał Żbikowski‡
Cranfield University, Defence Academy of the United Kingdom, Shrivenham, England SN6 8LA, United Kingdom

DOI: 10.2514/1.35311

The aerodynamic design of a flapping-wing micro air vehicle requires a careful study of the wing-design space to ascertain the best combination of parameters. Here, such wing design for hovering insectlike flapping flight is studied using a nonlinear unsteady aerodynamic model developed by the authors. The work is characterized, in particular, by the insights it provides into flapping-wing flows and the use it makes of these insights for aerodynamic design. This is the first of a two-part paper. The effects of wing kinematics on the aerodynamic performance of such flapping wings are investigated in this part by varying one parameter at a time; the effects of wing geometry are considered in part 2. It is found here that there are benefits in increasing flapping frequency and stroke amplitude and in advancing wing pitching rotation. Other important trends are also identified and practical considerations are noted. When possible, comparisons are also drawn with quasi-steady expectations and discrepancies are explained.

Nomenclature

c	=	chord length, m
$\bar{c}$	=	mean chord length (S/R), m
$\mathcal{D}$	=	drag, N
f	=	flapping frequency, Hz
k	=	reduced frequency ($f\bar{c}/2V$)
$\mathcal{L}$	=	lift, N
l	=	wingspan, m
$\mathcal{Q}$	=	torque, Nm
R	=	wing length, m
Re	=	Reynolds number
S	=	wing area, m^2
St	=	Strouhal number (fl/V)
s	=	number of semichords traveled
$\mathcal{T}$	=	thrust, N
V	=	velocity, m/s
α	=	pitch angle
ρ	=	fluid density, kg/m^3
Φ	=	stroke amplitude
ϕ	=	stroke angle

I. Introduction

AGILE flight inside buildings, caves, and tunnels is of significant military and civilian value and is an attractive application for micro air vehicles (MAVs), defined here as flying machines of the order of 150 mm in size. Indoor flight imposes particular design and performance requirements, including small size, low speed, hovering capability, high maneuverability at low speeds, and (for covert operations) small acoustic signature, among other things. As discussed elsewhere [1–4], insectlike flapping is a solution that meets these requirements and is proven in nature.

Received 26 October 2007; revision received 11 June 2008; accepted for publication 13 June 2008.

*Research Officer, Department of Aerospace, Power and Sensors. Member AIAA.

†Professor of Aeromechanical Systems, Department of Aerospace, Power and Sensors. Associate Fellow AIAA.

‡Reader in Control Engineering, Department of Aerospace, Power and Sensors. Member AIAA.

Although a number of elements characterize the design of a flapping-wing MAV, the focus here is on its wing aerodynamic design. This is crucial because for a flapping-wing MAV (FMAV) the wings are not only responsible for lift, but also for propulsion and maneuvers. Although insect flapping wings offer a proven solution and are abundant in nature (there are over 170,000 species of flying insects), little is known about the optimality of their wing design. Unlike for fixed or rotary wings, the parametric space associated with flapping wings is largely unexplored. A study that addresses the effects of both wing kinematics and wing geometry on the aerodynamic performance of flapping wings is required, and the former forms the underlying theme of this paper. The effect of wing geometry is considered elsewhere [5]. This work also provides insights into flapping-wing flow physics and uses these insights for aerodynamic design.

Although Ellington's [6] seminal work rejuvenated interest in insect flight, it is only recently that attention has been directed toward the design of vehicles that use insectlike flapping wings, particularly at the MAV scale [1–3]. In a later study, Ellington [7] proposed design guidelines based on scaling from nature, but this does not give physical insight or allow design optimization. Dickinson et al. [8] investigated the effect of advancing or delaying pitch rotation of the flapping wing with respect to its translational motion, using experiments on Dickinson's Robofly: a scaled-up mechanical model of the fruit fly *Drosophila*. Ramamurti and Sandberg [9] used a computational fluid dynamics (CFD) method to demonstrate this effect and presented some useful flow visualization. Sun and Tang [10] also used a CFD code to investigate the effect of advancing and delaying pitch rotation on insectlike flapping flight and the effect of varying the duration of stroke reversals [11]. In an earlier study [12], they investigated the effect of Reynolds number and the duration of wing stroke reversal. They also studied the effect of advance ratio (the ratio of flight speed to wing mean tip speed) in forward flapping flight [13]. Yu and Tong [14] used an aerodynamic modeling approach [15] to study forward flapping flight at various advance ratios by varying asymmetries between up- and downstrokes. However, none of the preceding studies aimed to produce an optimized wing aerodynamic design.

Milano and Gharib [16] made probably the only study thus far aimed at optimizing wing kinematics. They used a genetic algorithm paired with digital particle-image velocimetry experiments on a flapping wing in a water-filled towing tank. By using insectlike kinematics, they optimized for average lift over four flapping cycles and found a number of convergent solutions in the parameter space. They noted that the optimally efficient solutions all tended to generate leading-edge vortices of maximum strength. However, their

approach, as well as the others mentioned earlier, was limited in scope and, particularly, in providing physical insight into the flapping-wing flow. Such insight is crucial in explaining the forces observed and making informed decisions on wing aerodynamic design.

This is the first of a two-part paper [5]. The work presented in this part addresses the issue of converging on preferred design for a flapping wing in terms of wing kinematics. The parameters in the design space are varied one at a time to identify trends for optimizing wing performance and hence finding the best combination for an FMAV. It is part of an ongoing study at Cranfield University (Shrivenham) toward the aerodynamic design of insectlike flapping wings for MAVs. The work began with a preliminary investigation using a simple quasi-steady aerodynamic technique [17] followed by another employing a more advanced quasi-steady model [18]. Then, using the nonlinear unsteady aerodynamic model developed by Ansari et al. [19,20] for insectlike flapping wings in the hover, a more advanced investigation was conducted [21]. The current work is a further extension of this study and now considers the effects of a wider range of wing planforms and other wing-design parameters. This work also includes more detailed analysis based on considerations of flow physics in the flapping-wing regime and, in doing so, provides much-needed insight into the observed characteristics while making comparisons with corresponding quasi-steady predictions. In part 2 [5], the effects of wing geometry on flapping-wing design is considered.

To compare various configurations, some measure of performance is required. It is customary in fixed-wing aircraft studies to consider lift and lift-to-drag ratio for wing performance, whereas for rotorcraft, lift-to-torque ratio is also an important performance indicator, as it is a measure of power requirement. All of these are used here, albeit modified appropriately for flapping wings.

A. Insectlike Flapping

Insect flapping flight has been discussed extensively in [4] and only the features essential to this study are discussed here.

1. *Wing Kinematics*

The description given here is for the hover of two-winged flies (Diptera) (e.g., the fruit fly *Drosophila*), as they are easier to analyze and emulate and are excellent flyers. Insects use a reciprocating wing motion for flight, comparable to the sculling motion of the oars of a rowing boat. This may be decomposed into three component motions: sweeping (fore and aft movement), heaving or plunging (up and down movement), and pitching (varying incidence). Flapping frequency is typically in the range of 5–200 Hz, decreasing with increasing insect size and weight [22].

Each flapping cycle consists of two half-strokes: a downstroke and an upstroke (see Fig. 1). These are the translational phases of the flapping cycle, because the wings' linear motions dominate over rotational motions (changes in pitch). The downstroke refers to the motion of the wing from its rearmost and highest position (relative to the body) to its foremost and lowest position. The upstroke describes the return cycle. At either ends of the half-strokes, the rotational phases of the flapping cycle come into play: stroke reversal occurs, whereby the wing pitches rapidly and reverses direction for the subsequent half-stroke. During this process, the morphological lower surface becomes the upper surface and the leading edge always leads (Fig. 1).

During a half-stroke, the wing accelerates to a roughly constant speed around the middle of the half-stroke, before slowing down to rest at the end of it. The velocity during the wing-beat cycle is therefore nonuniform, and for hover, in particular, the translational motion (i.e., distance vs time) of the wing tip does not vary dramatically from a pure sinusoid [6]. Wing pitch seems to be relatively constant between stroke reversals (see [23]).

2. *Aerodynamic Phenomena*

The aerodynamics of insect flapping flight is too vast a subject to be addressed in great detail, and so only the most pertinent flow features in Diptera hover are addressed now. These features were employed in the development of the aerodynamic model used for the current parametric study [19,20]. The flow associated with insect flapping flight is incompressible, laminar, and unsteady and occurs at low Reynolds numbers. The unexpectedly large forces observed can be attributed to a combination of unsteady and vortical aerodynamic effects.

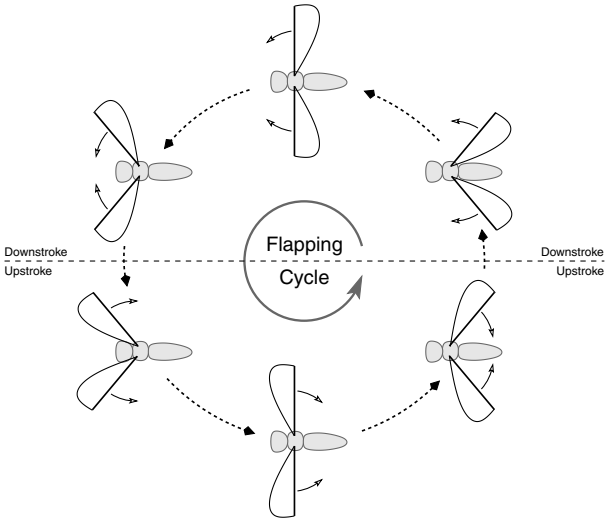

Fig. 1 Half-strokes during insect flapping (bold line marks the wing leading edge).

The main identifying feature of an insect's flapping cycle is the wing's start-stop-reversal behavior, and this is fundamental to the aerodynamics that make this flight regime possible. The starting vortices that are shed each time the wing starts are of the opposite sense to the bound circulation and have an inhibitory effect on lift: the so-called *Wagner effect* [24]. Although stroke reversals occur at the end of the half-strokes, there is still significant translational motion during their execution, and the increasing incidence results in an increase in lift: the so-called *Kramer effect* [25]. The converse is true at the start of the subsequent half-stroke when the wing rapidly pitches down.

As a flapping wing moves, it sets the surrounding air in motion. Additional force is required to overcome the repeated acceleration and deceleration of this mass of air: the so-called *apparent mass forces* [26], which must be accounted for. By the very nature of the kinematics, the fluid in the vicinity of the flapping wing is not quiescent (especially during hover or low-speed flight) and *wake capture* forces [27] arise as the wing regularly encounters its own shed wake.

By far, the most important aerodynamic mechanism in insect flight is the *leading-edge vortex* identified by Ellington et al. [28]. They reported that it persisted through each half-stroke and was responsible for the augmented lift forces. They also noted its spanwise-spiraling nature, although this has been questioned by Dickinson et al. [8]. Wu and Sun [12] showed that except for very low Reynolds numbers ($Re \lesssim 100$), the leading-edge vortex suffices as the high-lift mechanism for sustaining flight in insects.

A further feature of insectlike flapping flows is their dependence on the number of semichords traveled [18]. During the development of his model, Ansari [18] noted that in moving spanwise along a flapping wing, a phase difference in vortex-shedding patterns existed between wing sections. Flow in the outboard regions was more developed and older in terms of semichords traveled than the inboard regions. More mature flow, having traveled more semichords, was found to be more prone to vortex breakaway. A similar observation was made by Ellington et al. [28], who reported that vortex breakaway caused the leading-edge vortex to lift off the wing surface in the outboard regions of the wing. Wilkins and Knowles [29] also made a similar observation in their CFD study on impulsively started rotating wings. Vortex breakaway causes a reduction in lift but an increase in drag. Because outboard wing sections are most likely to

be affected, the implications for torque are significant. This behavior is crucial in explaining some of the trends observed in the parametric study presented in Sec. III. The link between flow behavior and flow age in terms of semichords traveled shows that a reduced-frequency-type parameter is still relevant in this form of unsteady flow and stresses the importance of preserving the Strouhal number [29] in experimental investigations, a point also highlighted in [4,20].

Although the model uses 2-D vortex breakaway to explain the variations in the forces observed, in 3-D viscous flow, this is in fact the result of Kelvin–Helmholtz instability in the vortex structures and the merging of the leading-edge vortex with the tip vortex [29]. However, as shown in the following section, the two mechanisms appear to give corresponding effects, and hence the model of Ansari et al. [19,20] is used in this study.

II. Nonlinear Unsteady Aerodynamic Model

Flapping-wing flows necessitate capturing the separated flow due to the leading-edge vortex and the trailing-edge wake and their complex interaction with the wing. To describe the problem for hover, Ansari et al. [19,20] developed an unsteady indicial model based on two novel coupled nonlinear (to accommodate the curvilinear wake, unlike Wagner's [24] linear function for a flat wake) integral equations. One of the equations models the leading-edge vortex and the other models the rest of the wake. Their coupling expresses the interaction and the nonlinearity captures wake deformation. The method does not rely on any ad hoc adjustments/corrections or on empirical fixes (as did many previous models [4]) and shows good agreement with the experiment (see Figs. 2–4). The interested reader is referred to [19,20] for full details on the model and its accuracy.

Given input kinematics and geometry, the model is capable of returning forces and moments as well as generating flow visualization (see Fig. 5). Such a model is a challenge, as it necessitates capturing the vortical phenomena and their interaction with the wing. Ansari et al. [20] validated their model for hover (see Figs. 2–4). Figure 4 shows how our aerodynamic model compares with the CFD model of Ramamurti and Sandberg [30]. The wing kinematics for the advanced and delayed cases have a lead and a lag, respectively, of 8% of the flapping cycle on the symmetrical case. Our model produces results that are consistent with the experimental data of Dickinson et al. [8], whereas the results of Ramamurti and Sandberg [30] compare well with the experimental data of Dickinson et al. [8] that they quote. As highlighted elsewhere [31], more experimental data are needed.

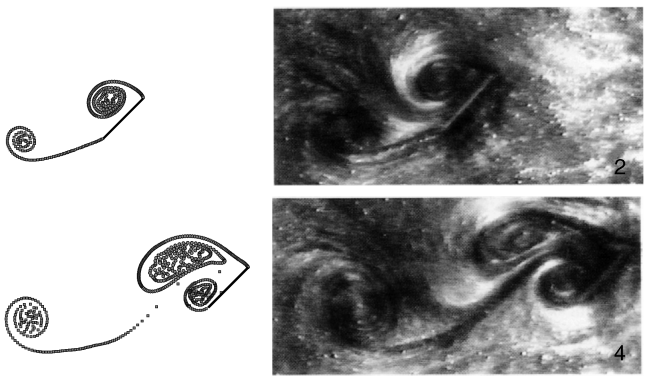

Fig. 2 Theoretical prediction [19,20] of 2-D flow-visualization compared with experimental data [33].

The model of Ansari et al. [20] has been shown to be among the best currently available [4]. For this reason, it was used here for the parametric study. A comprehensive review of other aerodynamic modeling methodologies (including CFD) can be found in [4].

Our model [19,20] is quasi-three-dimensional, using a blade-element method to divide the wing spanwise into chordwise strips using radial chords [17,19] (see Fig. 6) that are each treated essentially as two-dimensional. In the current study, the wing section is modeled as a rigid flat plate, but the model is capable of including camber and thickness. Although the insectlike flapping kinematics are spherical, the wings' plunging motion is usually small, and therefore our approach reduces the spherical geometry to a cylindrical one. As a result, each wing section resides in a radial cross plane that is unwrapped flat, and the flow is solved as a planar two-dimensional problem. The overall effect on the wing is obtained by integrating along the span. Because of its quasi-three-dimensional nature, there is no communication between adjacent sections. Hence, spanwise flow in the leading-edge vortex is not treated. The validity of this and the cylindrical-system approximation is discussed in [20]. The impact of neglecting 3-D viscous effects is addressed subsequently.

The aerodynamics were realized using potential flow methods. Because of flow separation from both leading and trailing edges, the Kutta–Joukowski condition is enforced there. The flow is assumed to be irrotational (except at solid boundaries and discontinuities in the wake), and the effects of viscosity are included indirectly in the form of the Kutta–Joukowski condition and in the formation and shedding of vortices. The solution is implemented numerically using a discrete vortex method, and a spin-off of this technique is that flow visualization is generated automatically. Forces and moments are computed by Kelvin's method of impulses [32], and the model was validated against flowfield [33] and force [8,23] experiments.

Some comment is required on certain 3-D flow features that are not captured by the aerodynamic model used here [19,20], notably the effects of the tip vortex, spanwise flow, and some aspects of viscosity. These are addressed now.

On finite wings with attached flow, the effect of the tip vortex is to reduce lift as air spills from the pressure side of the wing to the suction side. The forward motion of the wing means that a trailing vortex system is formed behind the wing. This induces a downwash on the wing, thereby reducing the effective angle of attack and thus decreasing lift. However, with suitable shaping of the tip, as in the British Experimental Rotor Program (BERP) helicopter rotor blades

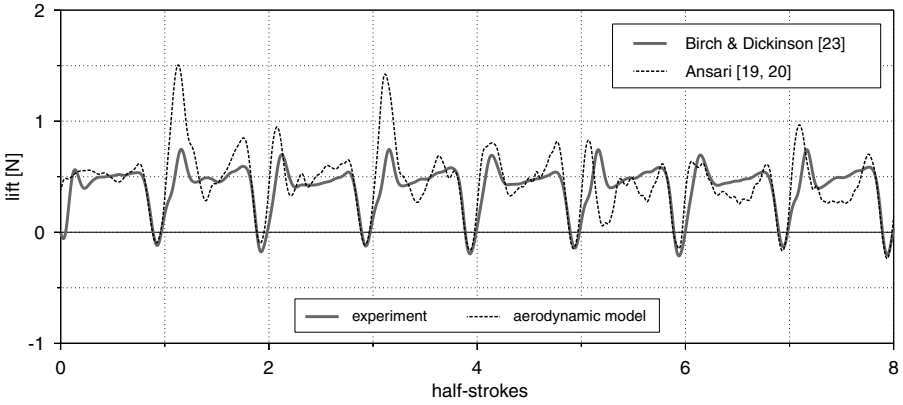

Fig. 3 Theoretical prediction [19,20] of lift force on a 3-D wing compared with experimental data [23].

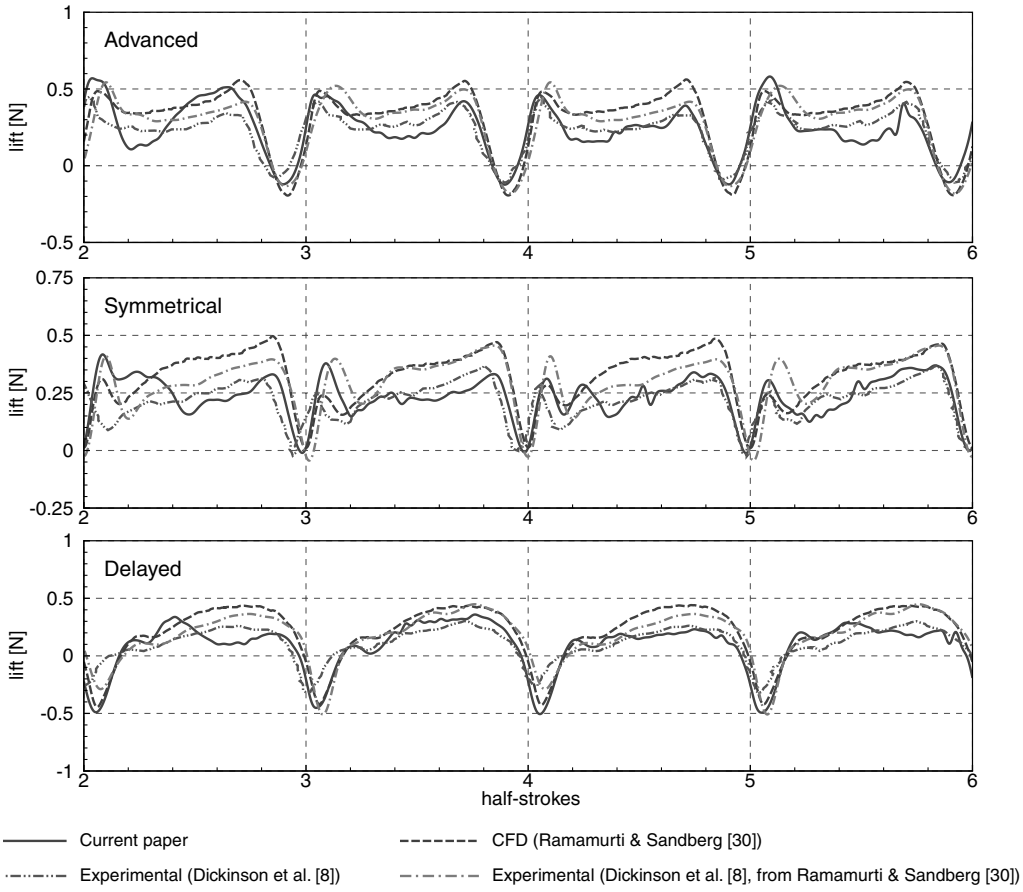

Fig. 4 Plot comparing results from the aerodynamic model used here [19,20] with CFD [30] and experimental measurements [8]. Results shown are for advanced, symmetrical and delayed kinematics.

[34–36], the tip vortex can be located to *improve* the lift force on the wing (i.e., by managing separated flow over the tips, lift can be improved). It is therefore difficult to identify an obvious effect of neglecting the tip vortex in our model, in which the flow is predominantly separated.

Experimental [28,37] and computational [29] observations have revealed that spanwise flow in the leading-edge vortex on a flapping wing improves its stability as vorticity is extracted toward the outboard regions. The quasi-3-D model used here does not model this feature, resulting in vorticity being transported chordwise only; the leading-edge vortex in each wing section tends to break away as more chord lengths are swept, which is a 2-D flow feature. Comparison with experimental data, however, shows that the breaking away produces slight oscillations about the measured values of forces (Figs. 3 and 4), thus giving confidence that the model is correctly capturing total circulation. Indeed, the creation of vorticity in the model is regulated strictly by satisfying the fluid dynamics equations for vorticity balance [19,20].

Aerodynamic modeling progresses from first principles and introduces several simplifications to the basic equations of fluid mechanics, justified by the flow phenomenology and/or geometric and kinematic symmetries [4]. Following this, some of the effects of viscosity are included in the current model, such as in the form of the Kutta–Joukowski conditions at the leading and trailing edges and in the formation of vortices shed into the wake. Normally, in inviscid flows, shed vortices are convected at the local flow velocities. In viscous flows, there is the additional effect of viscous diffusion [38–40] that is not modeled here, and neither is vortex stretching, which is encountered in 3-D flows [41–43]. In our model, vortices shed into the wake are only convected (according to the Biot–Savart law). It is

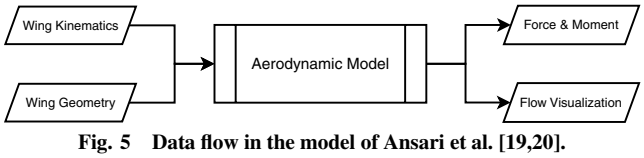

Fig. 5 Data flow in the model of Ansari et al. [19,20].

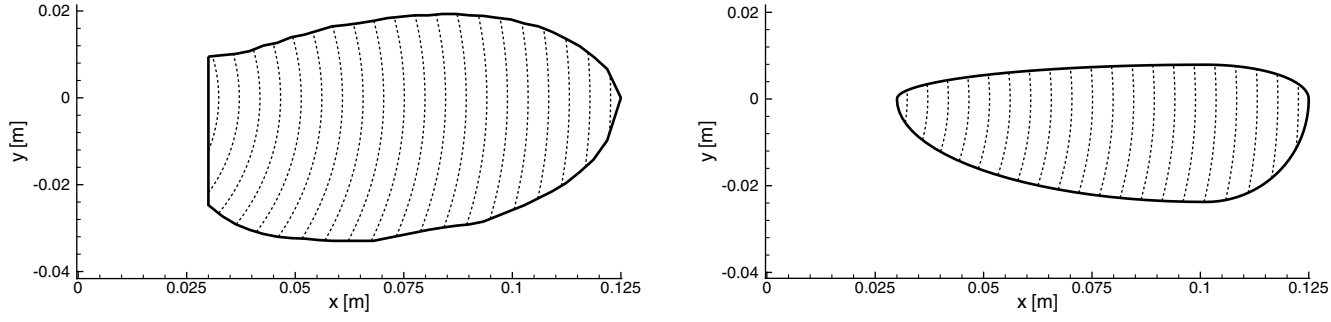

a) Robofly [8] **b) Four-ellipse (after Pedersen [44])**

Fig. 6 Planform shapes used for wing kinematics study (with radial chords shown).

difficult to quantify the net effect of neglecting diffusion and stretching. Although vortices that are far removed from the wing are less likely to have much influence, most vortices shed in the hover are in close proximity to the wing and may have greater impact on the flow and hence on forces and moments. Further, in their CFD studies on insect flight, Ramamurti and Sandberg [9,30] showed that viscous effects are indeed minimal, even at Reynolds numbers as low as $Re = 120$; the translational and rotational mechanisms in insectlike flapping appear to dominate the forces observed.

With the aforementioned caveats, our aerodynamic model can be used with some confidence as a tool for the study presented here, in view of the fact that there is no single clear effect of neglecting these flow features and, more important, because the agreement with experimental data is very encouraging [flow phenomenology, magnitude of the forces, and their unsteadiness are all captured well (see Figs. 2–4)].

III. Wing Kinematics Study

In what follows, the simulations were run with one wing and the overall effect was obtained by doubling this contribution.[§] In doing so, symmetry was assumed and any interference effects of the other wing were ignored. This seems to be a reasonable assumption for insectlike hover. The fluid medium used was air at standard sea-level atmospheric conditions (density $\rho = 1.225\ \mathrm{kg/m^3}$). The wing sections were assumed to be thin and flat with no flexion. The required wing kinematics and wing geometry parameters were used as input to the program, and the resulting forces (and related parameters) generated were the outputs used for the comparisons.

Because of the nature of the flapping wing (and the associated continuously varying forces), the measures used for comparison were mean lift $\mathcal{L}$ and mean drag $\mathcal{D}$ (these were averaged over the four half-strokes for which most simulations were run). From a wing-design perspective, an even better measure is mean lift-to-torque ratio $\mathcal{L}/\mathcal{Q}$, as it gives an indication of power requirement. This was also used, together with mean lift-to-drag ratio $\mathcal{L}/\mathcal{D}$ in some cases. When appropriate, plots showing variations in the center of drag (the spanwise radial position at which the resultant drag $\mathcal{D}$ acts) were also included. These were deduced from the ratio of $\mathcal{L}/\mathcal{D}$ to $\mathcal{L}/\mathcal{Q}$.

Unlike the study on wing geometry [5], where wing kinematics are fixed and wing geometry is varied, the approach here relies on fixing wing geometry and studying the effect of variations in parameters relating to wing kinematics. The response of insectlike flapping wings to the effects of changing wing kinematics parameters was investigated using two given wing planform shapes (see Fig. 6) so that the independence of wing kinematics effects from wing shape could be established. The wing planforms used were a scaled-down version of the Robofly used in the validation of the model (Fig. 6a) and a wing shape derived from four elliptical arcs [dubbed four-ellipse (see Fig. 6b)].

The parameters in the design space are varied one at a time to identify trends for optimizing wing performance and hence finding the best combination for an FMAV. The remaining parameters were maintained at the values shown in Table 1. The sweep $(\phi, \dot{\phi})$ and pitch $(\alpha, \dot{\alpha})$ time histories used were those provided by Birch and Dickinson [23] from his Robofly experiments (see Fig. 7). The locus of the wing-tip path was a flat figure eight with no heave. Because the investigation in this section relates to kinematics, wing shape is of little consequence and two reference shapes were used (Fig. 6). Of greater importance is the manner in which the wing moves. The stroke amplitude Φ swept by the Robofly wing was computed as the maximum possible without interfering with the other wing (see Fig. 8 and associated discussion in Sec. III.B). The kinematics parameters studied were flapping frequency, stroke amplitude, and rotation phase. Because we limit ourselves to hover, the effect of advance ratio is not considered.

[§]In reality, if the wings come in close proximity to one another, some form of mutual interference would come into play, and hence the effect of two wings would not necessarily be the doubling of the single-wing forces.

Table 1 Standard wing kinematics parameters for simulations

Parameter	Value
Flapping frequency	2 Hz
Stroke amplitude	Maximum possible (Fig. 8)
Wing motion	Dickinson et al. [8] (Fig. 7)
Rotation phase	Advanced by 6% of cycle

A. Flapping Frequency

Flapping frequency refers to the number of complete wing beats (downstroke and upstroke) per second and is the most visible kinematic characteristic in insects. The study presented here shows the effect that flapping frequency has on lift, drag, and other aerodynamic characteristics. In Fig. 9, the mean lift and mean drag characteristics for the two planforms considered are shown, and a power-law fit was drawn to connect the individual points. As would be expected, both mean forces increase with flapping frequency f because, for a fixed stroke amplitude, the wings travel faster. Because aerodynamic forces scale with the square of the velocity, the trend seen in Figs. 9a and 9b is roughly proportional to f^2.

In fact, the power on f is slightly less than 2 because of the shed wake, especially the compounded effect of the vortices shed at stroke reversal. (These are the stopping vortices from the previous half-stroke and the starting vortices from the current half-stroke.) This effect is more pronounced for the Robofly wing than it is for the four-ellipse one (cf. Figs. 9a and 9b). The four-ellipse wing has smaller chords and hence sweeps longer arcs ($\sim$143.5 deg); therefore, it escapes to greater distances from the wake shed at stroke reversal. The Robofly wing, on the other hand, is quite the opposite: it has longer chords and sweeps shorter arcs ($\sim$101.7 deg), thereby remaining in the vicinity of the near shed wake and hence experiencing more inhibitory effects.

Higher flapping frequencies f are therefore beneficial because they increase lift without a corresponding change in lift-to-torque ratio (the latter depends mainly on wing planform, which was unchanged in these experiments). However, an upper limit might be set on f, provided by the requirement to keep the flapping wing inaudible[¶] ($\lesssim$20 Hz). Another practical constraint is mechanical hysteresis: as flapping frequency increases, the hysteresis may lead to increasing power losses.

B. Stroke Amplitude

Stroke amplitude was computed from the maximum angle that could be swept by the wing within a semicircle without crossing the symmetry plane (see Fig. 8). For one half-stroke, the maximum angle that can be swept is $\phi_1 + \phi_2$. At the end of the half-stroke, stroke reversal causes the angles ϕ_1 and ϕ_2 to be interchanged and the situation in Fig. 8 is reversed. Therefore, to avoid collision with the other wing, it is necessary that the sweep *extents* do not exceed the smaller of ϕ_1 and ϕ_2 in any half-stroke so that the leading and trailing edges never cross the line of symmetry (vertical axis in Fig. 8). The maximum possible stroke amplitude Φ was therefore computed as $\Phi = 2\ \min(\phi_1, \phi_2)$. For this investigation, the stroke amplitude was varied from small values up to the maximum possible, as described by the preceding equation. The results from the study are now discussed.

The effect of varying Φ on mean lift and mean drag is shown in Fig. 10. Because the simulations were run for the same frequency, increasing stroke amplitude required that a greater arc be swept by the flapping wing in the same time (hence, higher velocities). From a quasi-steady perspective, a result similar to that obtained for the preceding flapping frequency (Fig. 9) would be expected. However, closer inspection of Figs. 10a and 10b reveals that the relationship is more linear than quadratic. This is explained subsequently.

In the notation of Wagner [24], as the length of the stroke increases, so does the number of semichords traveled s. Wing

[¶]In practice, there will also be the added noise of the mechanism exciting the wing into flapping motion.

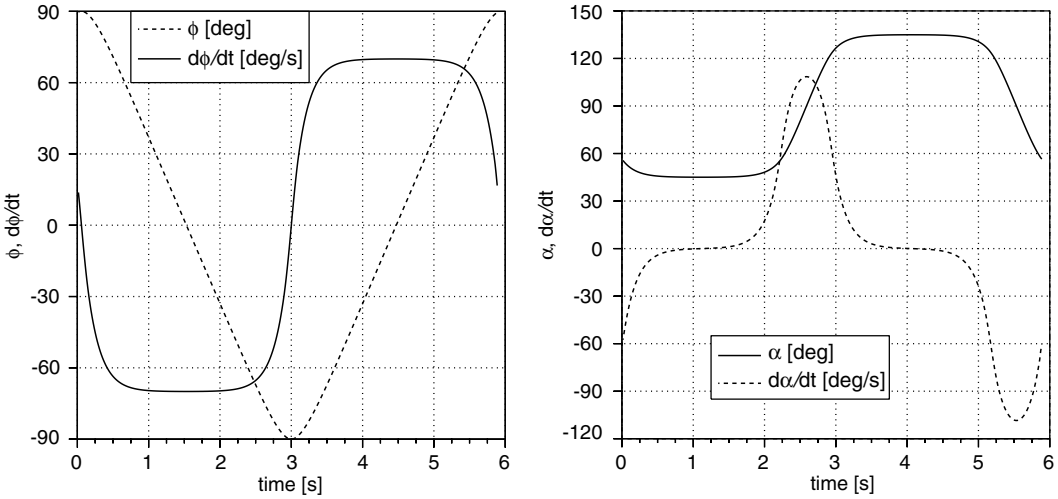

a) Sweep characteristics **b) Pitch characteristics**

Fig. 7 Kinematics of Dickinson's Robofly showing sweep ($\phi, \dot{\phi}$) and pitch ($\alpha, \dot{\alpha}$) characteristics for one cycle.

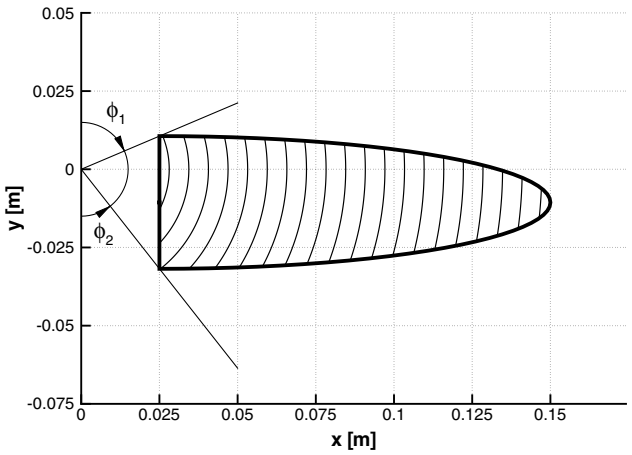

Fig. 8 Calculating stroke amplitude from sweep angles.

sections that have traveled more semichords have more developed flowfields and are more prone to vortex breakaway (especially in the leading-edge vortex), which curbs the growth of lift and drag. Therefore, the effect of increasing velocity accompanying increasing stroke amplitude is partly offset by the flow being more developed (and partially breaking away).

Because the flow physics appear to change as stroke amplitude is varied, it may be expected that there would be a corresponding effect on mean lift-to-drag $\mathcal{L}/\mathcal{D}$ and mean lift-to-torque $\mathcal{L}/\mathcal{Q}$ characteristics. These are shown in Fig. 11. An examination of $\mathcal{L}/\mathcal{Q}$ for the simulations explains the less-than-quadratic appearance of the lift $\mathcal{L}$ and drag $\mathcal{D}$ plots noted earlier. For the Robofly wing (Fig. 11a), there is a general increase in $\mathcal{L}/\mathcal{Q}$ with stroke amplitude until it peaks at around 90 deg. This peak represents the situation in which the stroke length is long enough to enable high lift and yet short enough to avoid major flow breakaway (and the associated loss of lift).

The results for the four-ellipse wing (Fig. 11b) show a slightly different behavior: there is little change in $\mathcal{L}/\mathcal{Q}$ with stroke amplitude (as would be expected from quasi-steady considerations). Because of the small chord lengths, the flow matures more quickly and it is increasingly costly to sweep bigger arcs.

From $\mathcal{L}/\mathcal{Q}$ and $\mathcal{L}/\mathcal{D}$, an indication of the center of drag along the wingspan can be estimated.** Whereas the four-ellipse wing generates most drag in the range of 74–76% span for all stroke amplitudes considered (see Fig. 12), the center of drag for the Robofly wing generally moves outboard as stroke amplitude increases [in the range of 62–70% span (Fig. 12)]. This means that outboard sections become increasingly "draggy" as longer arcs are swept. The drop in chord length for the Robofly wing is more gradual than it is for the four-ellipse wing. Hence, more of its outboard sections suffer from the effect of sweeping large arcs (and hence semichords traveled s). In the case of the four-ellipse wing, most of the outboard wing sections experience flow breakaway, even for small stroke amplitudes, due to their small chord lengths. Therefore, increases in stroke amplitude do not exacerbate their drag characteristics by much and the wing appears to be little affected.

**From the definition of torque $\mathcal{Q}$, radial distance of center of drag is $(\mathcal{L}/\mathcal{D})/(\mathcal{L}/\mathcal{Q})$.

C. Rotation Phase

The rotational (pitching) phases of insectlike flapping may not be synchronized with the translational phases, so that stroke reversals are not symmetrical about the translational phases of the cycle; that is, a phase lead or lag may exist between the two (see Fig. 13). The study presented in this section shows the effect of advancing or delaying rotation on the lift, drag, and related characteristics.

The kinematics used are based on those provided by Dickinson et al. [8] (see Fig. 7) but with phase lead or lag introduced. In fact, in Dickinson et al.'s kinematics, rotation led translation by 6% of the flapping cycle; these kinematics have been used in the other preceding studies. Here, these were modified to 0% lead (or lag) before the desired amounts of lead or lag were introduced. A lead or lag of 0% refers to the symmetric condition in which the wing is vertical (angle of attack $\alpha = 90$ deg) at the end of the half-stroke when the translational motion of the wing ceases momentarily before restarting in the opposite direction (Fig. 13b). Advanced rotation (lead) means that this orientation occurs earlier, before the wing has come to a stop (Fig. 13a). Conversely, in a delayed rotation (lag), the wing reaches the vertical position after the next half-stroke has begun (Fig. 13c).

Results for mean lift and mean drag are shown in Fig. 14. For both the Robofly and four-ellipse wings, the best lift characteristics are obtained when stroke reversals have a lead of about 5% of the flapping period on the translational motion; that is, the flapping wing begins pitching up for stroke reversal early so that most of the rotational phase is complete by the start of the subsequent half-stroke. The behavior can be understood by considering the time-history of lift (see Fig. 15). In the case of advanced rotation, the wing pitches to a high angle of attack, although the translational velocity is still significant. This results in an increase in the quasi-steady component of lift and hence total lift (Fig. 15a); this is a manifestation of the Kramer effect, explained in Sec. I.A.2.

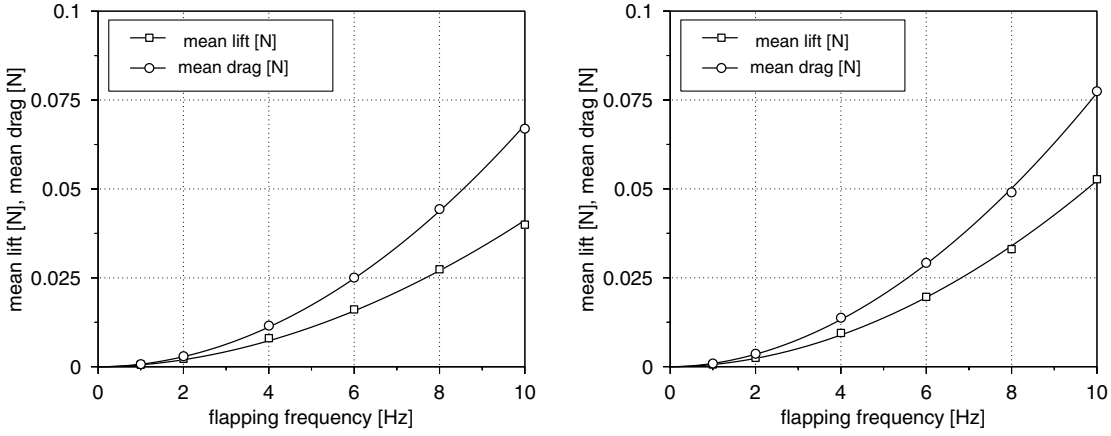

a) Robofly **b) Four-ellipse**

Fig. 9 Effect of flapping frequency on mean lift and drag.

This benefit of advancing pitching rotation comes with limited returns, due to the inhibitory effects of the starting vortex that accompanies the high angle of attack. Consider, for example, the case in which rotation leads translation by 10% of the flapping cycle (Fig. 14). Stroke reversal begins much earlier than in the case of a 5% lead so that the translational velocity is higher, and so the accompanying starting vortex that is shed is stronger. As the wing subsequently slows, a weaker stopping vortex is also shed, and so the resultant effect is a decrease in lift. The case of 5%-advanced rotation therefore offers the best compromise for advancing pitching rotation and yet sheds a small enough starting vortex to give the best increment in lift.

As pitching rotation is delayed, the wing is increasingly facing the wrong way ($\alpha > 90$ deg) at the start of the next half-stroke, which results in high drag (Fig. 15b) and low lift (Fig. 15a). This is the other extreme of the Kramer effect, whereby a wing reducing angle of

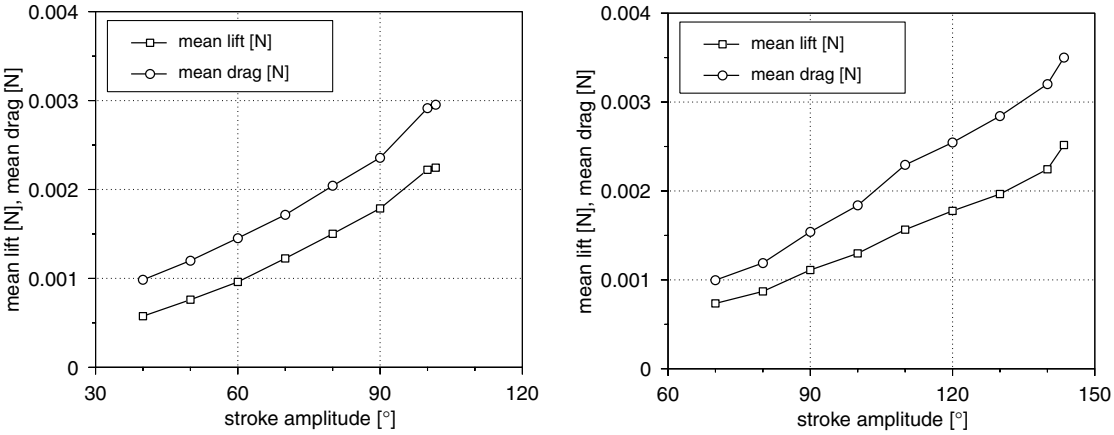

a) Robofly **b) Four-ellipse**

Fig. 10 Effect of stroke amplitude on mean lift and drag.

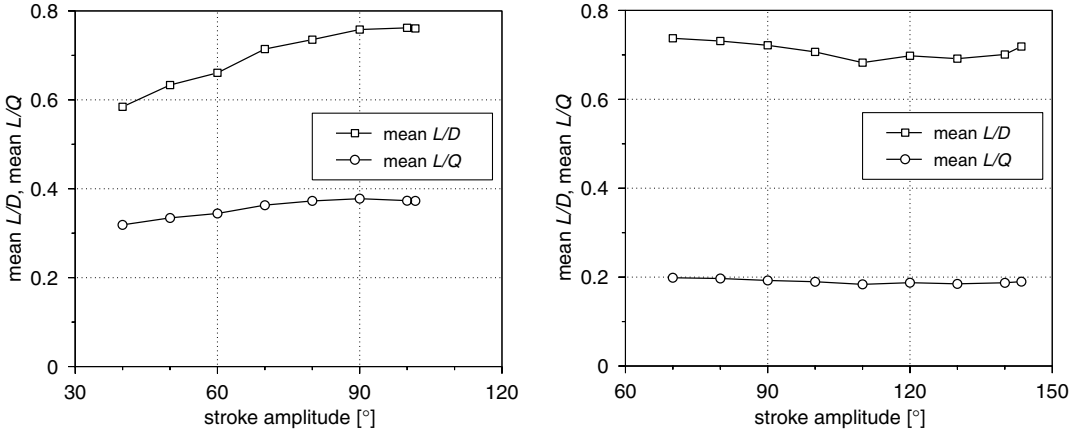

a) Robofly **b) Four-ellipse**

Fig. 11 Effect of stroke amplitude on mean lift-to-drag ratio $\mathcal{L}/\mathcal{D}$ and mean lift-to-torque ratio $\mathcal{L}/\mathcal{Q}$.

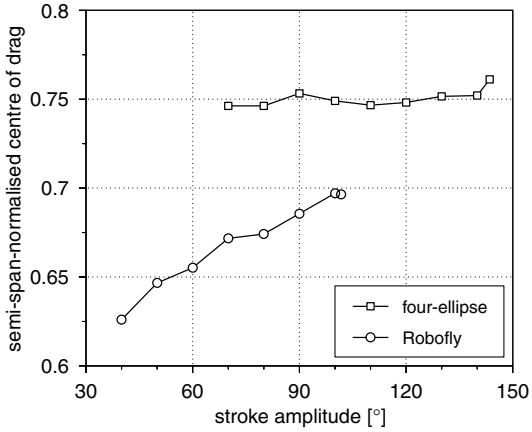

Fig. 12 Effect of stroke amplitude on normalized radial position (0 = root, 1 = tip) of center of drag for the Robofly and four-ellipse wings.

attack experiences a dynamic loss of lift. The late onset of stroke reversals means that smaller peaks in lift are observed at the end of the half-stroke and much bigger negative spikes follow at the start of the subsequent half-strokes.

From Fig. 14, it can also be seen that mean drag generally increases as rotation is advanced. Therefore, from a wing-design perspective, the best compromise may not be high lift alone, but rather high lift-to-drag $\mathcal{L}/\mathcal{D}$ or high lift-to-torque $\mathcal{L}/\mathcal{Q}$ ratios. These are shown in Fig. 16. The best $\mathcal{L}/\mathcal{Q}$ characteristics are obtained for a phase lead of 2.5%, but this is not significantly better than that at a 5% lead. Because the lift for a phase lead of 2.5% is noticeably less than that at 5% (Fig. 14), the best combination of lift and lift-to-torque ratio for these kinematics occurs when pitching rotation has about a 5% lead on translation.

The fact that both the Robofly and four-ellipse wings show very similar trends indicates that the effects of rotation phase may be independent of wing geometry.

IV. Conclusions

A study of the effects of wing kinematics on the aerodynamic performance of insectlike flapping wings in the hover was presented. It is found that lift and drag increase with flapping frequency and stroke amplitude, but these increases are limited by practical considerations. Increases in lift and drag can also be achieved by advancing wing rotation so that stroke reversals begin (and end) earlier in a flapping cycle. This, however, has limited returns, due to the opposing effects of increased lift due to the Kramer effect and the inhibitory effect of the vortices shed during advanced pitching rotation and because the wing is increasingly facing the wrong way at the start of the subsequent half-stroke as stroke reversal is advanced.

Most of the studies were compared with quasi-steady predictions, and discrepancies were observed that were mainly attributed to the losses associated with the dependence of vortex shedding on the number of semichords traveled s by the wing sections (in reality, these would be due to 3-D effects, including Kelvin–Helmholtz instabilities and interference between the leading-edge vortex and the tip vortex). Large values of s were accompanied by a decrease in lift and an increase in drag, giving an overall reduction in aerodynamic performance.

In general, variations in wing kinematics are more difficult to implement mechanically than variations in a wing's planform shape. Therefore, it is of great interest to investigate whether desired

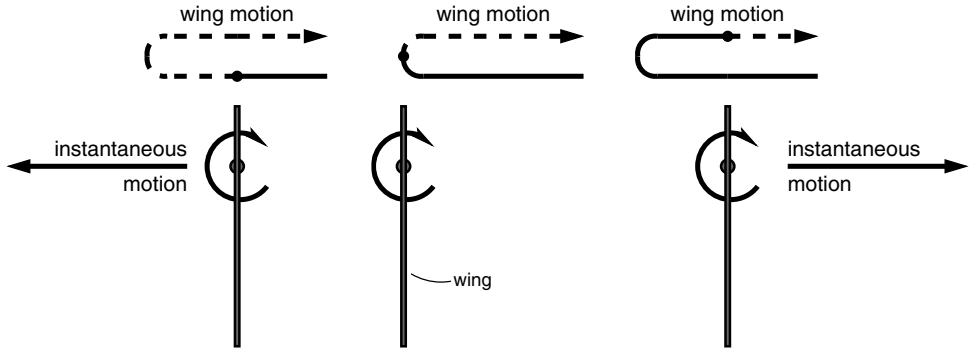

a) Advanced **b) Symmetric** **c) Delayed**

Fig. 13 Phase lead, symmetry, or lag determined by direction of wing motion when wing is vertical (the ● symbol between the solid and chain lines on the wing motion trace indicates the position at which the wing is vertical).

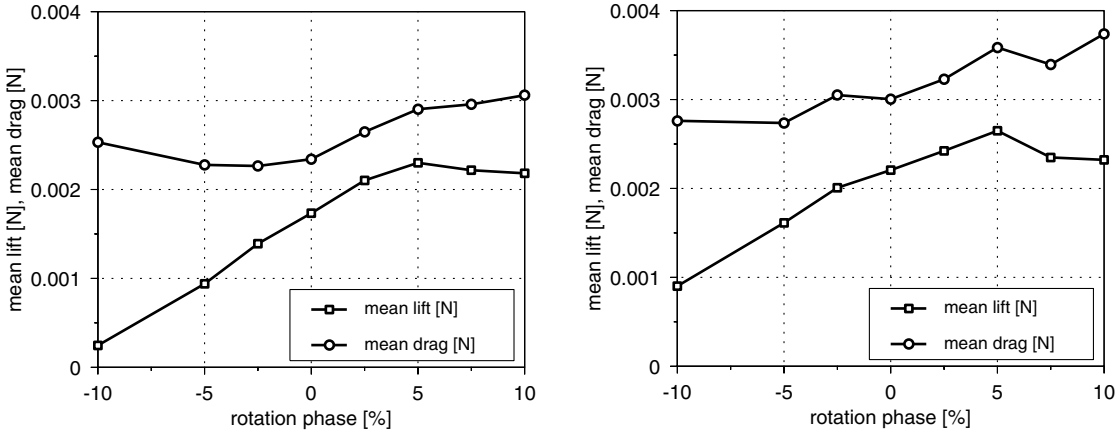

a) Robofly **b) Four-ellipse**

Fig. 14 Effect of rotation lead (+) or lag (−) on mean lift and mean drag.

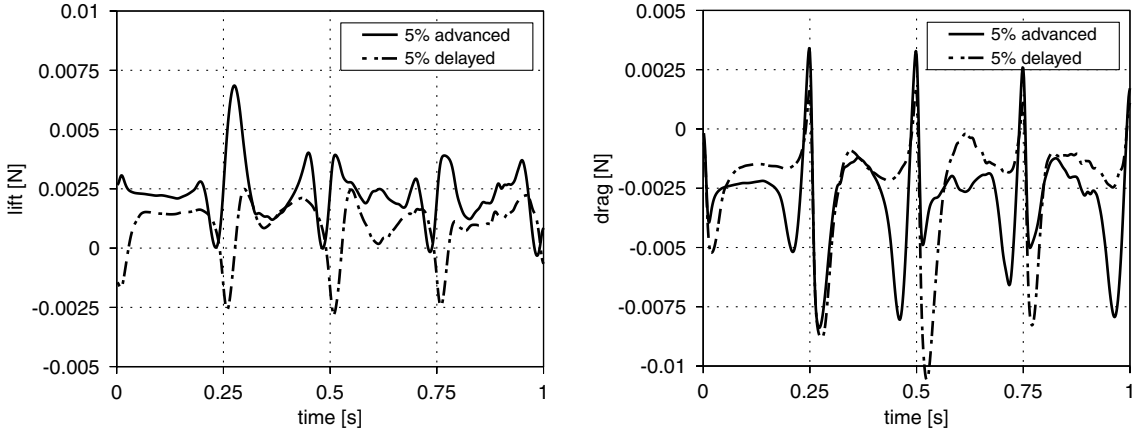

a) Lift **b) Drag**

Fig. 15 Lift and drag time-histories for the Robofly wing with advanced and delayed rotation calculated with our model [19,20]. The general shapes of these plots are in agreement with the experimental results of Dickinson et al. [8] (Fig. 2), and the CFD predictions of Sun and Tang [10] (Fig. 3) and Ramamurti and Sandberg [30] (Figs. 10 and 12).

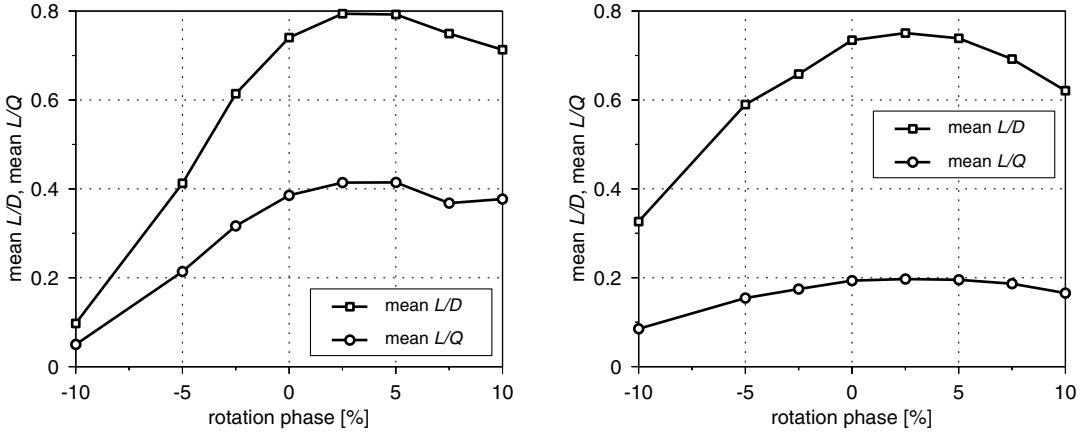

a) Robofly **b) Four-ellipse**

Fig. 16 Effect of rotation lead (+) or lag (−) of lift-to-drag ratio $\mathcal{L}/\mathcal{D}$ and lift-to-torque ratio $\mathcal{L}/\mathcal{Q}$.

aerodynamic design characteristics can be achieved by varying wing geometry rather than changing wing kinematics. A study of the effects of wing geometry parameters is required first and this is tackled in a separate study [5].

Acknowledgments

This work was supported by the Engineering and Physical Sciences Research Council through grants GR/M78472/01 and GR/S23025/01 and by the United Kingdom Ministry of Defence under the Joint Grants Scheme. The authors would also like to thank Michael Dickinson of the California Institute of Technology, Pasadena, CA, for the experimental force data used for validation of the aerodynamic model.

References

[1] Żbikowski, R., "Flapping Wing Autonomous Micro Air Vehicles: Research Programme Outline," *Fourteenth International Conference on Unmanned Air Vehicle Systems*, Bristol Univ., Bristol, England, U.K., 1999, pp. 38.1–38.5.

[2] Żbikowski, R., "Flapping Wing Micro Air Vehicle: A Guided Platform for Microsensors," *Royal Aeronautical Society Conference on Nanotechnology and Microengineering for Future Guided Weapons*, Royal Aeronautical Society, London, 1999, pp. 1.1–1.11.

[3] Żbikowski, R., "Flapping Wing Technology," *European Military Rotorcraft Symposium*, Royal Military College of Science, Shrivenham, England, U.K., 21–23 Mar. 2000, pp. 1–7.

[4] Ansari, S. A., Żbikowski, R., and Knowles, K., "Aerodynamic Modelling of Insectlike Flapping Flight for Micro Air Vehicles," *Progress in Aerospace Sciences*, Vol. 42, No. 2, Feb. 2006, pp. 129–172. doi:10.1016/j.paerosci.2006.07.001

[5] Ansari, S. A., Knowles, K., and Żbikowski, R., "Insectlike Flapping Wings in the Hover Part 2: Effect of Wing Geometry," *Journal of Aircraft*, Vol. 45, No. 6, 2008, pp. 1976–1990. doi:10.2514/1.35697

[6] Ellington, C. P., "The Aerodynamics of Hovering Insect Flight," *Philosophical Transactions of the Royal Society of London, Series B: Biological Sciences*, Vol. 305, Feb. 1984, pp. 1–181. doi:10.1098/rstb.1984.0049

[7] Ellington, C. P., "The Novel Aerodynamics of Insect Flight: Applications to Micro-Air Vehicles," *Journal of Experimental Biology*, Vol. 202, No. 23, 1999, pp. 3439–3448.

[8] Dickinson, M. H., Lehmann, F.-O., and Sane, S. P., "Wing Rotation and the Aerodynamic Basis of Insect Flight," *Science*, Vol. 284, June 1999, pp. 1954–1960. doi:10.1126/science.284.5422.1954

[9] Ramamurti, R., and Sandberg, W. C., "A Three-Dimensional Computational Study of the Aerodynamic Mechanisms of Insect Flight," *Journal of Experimental Biology*, Vol. 205, No. 10, 2002, pp. 1507–1518.

[10] Sun, M., and Tang, J., "Lift and Power Requirements of Hovering Flight in Drosophila Virilis," *Journal of Experimental Biology*, Vol. 205, No. 16, 2002, pp. 2413–2427.

[11] Wu, J., and Sun, M., "The Influence of the Wake of a Flapping Wing on the Production of Aerodynamic Forces," *Acta Mechanica Sinica*, Vol. 21, No. 5, 2005, pp. 411–418. doi:10.1007/s10409-005-0064-4

[12] Wu, J. H., and Sun, M., "Unsteady Aerodynamic Forces of a Flapping Wing," *Journal of Experimental Biology*, Vol. 207, No. 7, 2004, pp. 1137–1150.
doi:10.1242/jeb.00868

[13] Sun, M., and Wu, J. H., "Aerodynamic Forces Generation and Power Requirements in Forward Flight in a Fruit Fly with Modeled Wing Motion," *Journal of Experimental Biology*, Vol. 206, No. 17, 2003, pp. 3065–3083.
doi:10.1242/jeb.00517

[14] Yu, Y., and Tong, B., "A Flow Control Mechanism in Wing Flapping with Stroke Asymmetry During Insect Forward Flight," *Acta Mechanica Sinica*, Vol. 21, No. 3, 2005, pp. 218–227.
doi:10.1007/s10409-005-0032-z

[15] Yu, Y., Tong, B., and Ma, H., "An Analytic Approach to Theoretical Modeling of Highly Unsteady Viscous Flow Excited by Wing Flapping in Small Insects," *Acta Mechanica Sinica*, Vol. 19, No. 6, Dec. 2003, pp. 508–516.
doi:10.1007/BF02484543

[16] Milano, M., and Gharib, M., "Uncovering the Physics of Flapping Flat Plates with Artificial Evolution," *Journal of Fluid Mechanics*, Vol. 534, June 2005, pp. 403–409.
doi:10.1017/S0022112005004842

[17] Ansari, S. A., Knowles, K., and Żbikowski, R., "Aerodynamic Modelling of Some Planforms for Insectlike Flapping Wings," *CEAS Aerospace Aerodynamics Conference*, Royal Aeronautical Society, London, 10–12 June 2003, pp. 38.1–38.14.

[18] Ansari, S. A., "A Nonlinear Unsteady, Aerodynamic Model for Insectlike Flapping Wings in the Hover with Micro Air Vehicle Applications," Ph.D. Thesis, Cranfield Univ., Shrivenham, England, U.K., Sept. 2004.

[19] Ansari, S. A., Żbikowski, R., and Knowles, K., "Non-Linear Unsteady Aerodynamic Model for Insectlike Flapping Wings in the Hover, Part 1: Methodology and Analysis," *Proceedings of the Institution of Mechanical Engineering, Part G: Journal of Aerospace Engineering*, Vol. 220, No. 2, 2006, pp. 61–83.
doi:10.1243/09544100JAERO49

[20] Ansari, S. A., Żbikowski, R., and Knowles, K., "Non-Linear Unsteady Aerodynamic Model for Insectlike Flapping Wings in the Hover, Part 2: Implementation and Validation," *Proceedings of the Institution of Mechanical Engineering, Part G: Journal of Aerospace Engineering*, Vol. 220, No. 3, 2006, pp. 169–186.
doi:10.1243/09544100JAERO50

[21] Ansari, S. A., Knowles, K., and Żbikowski, R., "Design Guidelines for Flapping-Wing Micro UAVs," *SAE 2005 Transactions: Journal of Aerospace*, Mar. 2006, pp. 1–10; also Society of Automotive Engineers Paper 2005-01-3197, 2005.

[22] Azuma, A., *The Biokinetics of Flying and Swimming*, Springer–Verlag, Berlin, 1992.

[23] Birch, J. M., and Dickinson, M. H., "The Influence of Wing-Wake Interactions on the Production of Aerodynamic Forces in Flapping Flight," *Journal of Experimental Biology*, Vol. 206, No. 13, 2003, pp. 2257–2272.
doi:10.1242/jeb.00381

[24] Wagner, H., "Über die Entstehung des Dynamischen Aufftriebes von Tragflügeln," *Zeitschrift für Angewandte Mathematik und Mechanik*, Vol. 5, No. 1, Feb. 1925, pp. 17–35.
doi:10.1002/zamm.19250050103

[25] Kramer, M., "Die Zunahme des Maximalauftriebes von Tragflügeln bei Plötzlicher Anstellwinkelvergrösserung (Böeneffekt)," *Zeitschrift für Flugtechnik und Motorluftschiffahrt*, Vol. 23, No. 7, Apr. 1932, pp. 185–189; also "Increase in the Maximum Lift of an Airfoil due to a Sudden Increase in Its Effective Angle of Attack Resulting from a Gust," NACA TM-678, 1932.

[26] Massey, B., *Mechanics of Fluids*, 7th ed., Stanley Thornes, Cheltenham, England, U.K., 1998.

[27] Dickinson, M. H., "The Effects of Wing Rotation on Unsteady Aerodynamic Performance at Low Reynolds Numbers," *Journal of Experimental Biology*, Vol. 192, No. 1, 1994, pp. 179–206.

[28] Ellington, C. P., van den Berg, C., Willmott, A. P., and Thomas, A. L. R., "Leading-Edge Vortices in Insect Flight," *Nature*, Vol. 384, Dec. 1996, pp. 626–630.
doi:10.1038/384626a0

[29] Wilkins, P., and Knowles, K., "Investigation of Aerodynamics Relevant to Flapping-Wing Micro Air Vehicles," 18th AIAA Computational Fluid Dynamics Conference, AIAA, Reston, VA, June 2007, pp. 1–13; also AIAA Paper 2007-4338, 2007.

[30] Ramamurti, R., and Sandberg, W. C., "Computational Study of 3-D Flapping Foil Flows," 39th AIAA Aerospace Sciences Meeting and Exhibit, AIAA Paper 2001-0605, Reno, NV, Jan. 2001.

[31] Żbikowski, R., Ansari, S. A., and Knowles, K., "On Mathematical Modelling of Insect Flight Dynamics in the Context of Micro Air Vehicles," *Bioinspiration & Biomimetics*, Vol. 1, No. 2, 2006, pp. R26–R37.
doi:10.1088/1748-3182/1/2/R02

[32] Thomson, W. H., "On Vortex Motion," *Transactions of the Royal Society of Edinburgh*, Vol. 25, 1869, pp. 217–260.

[33] Dickinson, M. H., and Götz, K. G., "Unsteady Aerodynamic Performance of Model Wings at Low Reynolds Numbers," *Journal of Experimental Biology*, Vol. 174,No. 1, 1993, pp. 45–64.

[34] Brocklehurst, A., and Duque, E. P. N., "Experimental and Numerical Study of the British Experimental Rotor Programme Blade," AIAA 8th Applied Aerodynamics Conference, AIAA Paper 1990-3008, Portland, OR, Aug. 1990.

[35] Duque, E. P. N., "A Numerical Analysis of the British Experimental Rotor Program Blade," *Journal of the American Helicopter Society*, Vol. 37, No. 1, Jan. 1992, pp. 46–54.

[36] Srinivasan, G. R., Raghavan, V., and Duque, E. P. N., "Flowfield Analysis of Modern Helicopter Rotors in Hover by Navier–Stokes Method," *Journal of the American Helicopter Society*, Vol. 38, No. 3, July 1993, pp. 3–13.

[37] Ellington, C. P., "Insects Versus Birds: The Great Divide," 44th AIAA Aerospace Sciences Meeting and Exhibit, Reno, NV, AIAA Paper 2006-0035, Jan. 2006.

[38] Saffman, P. G., *Vortex Dynamics*, Cambridge Monographs on Mechanics and Applied Mathematics, Cambridge Univ. Press, Cambridge, England, U.K., 1992.

[39] Cottet, G.-H., and Koumoutsakos, P. D., *Vortex Methods: Theory and Practice*, Cambridge Univ. Press, Cambridge, England, U.K., 2000.

[40] Majda, A. J., and Bertozzi, A. L., *Vorticity and Incompressible Flow*, Cambridge Texts in Applied Mathematics, Cambridge Univ. Press, Cambridge, England, U.K., 2002.

[41] Ploumhans, P., Winckelmans, G. S., Salmon, J. K., Leonard, A., and Warrene, M. S., "Vortex Methods for Direct Numerical Simulation of Three-Dimensional Bluff Body Flows: Application to the Sphere at $Re = 300$, 500, and 1000," *Journal of Computational Physics*, Vol. 178, No. 2, 2002, pp. 427–463.
doi:10.1006/jcph.2002.7035

[42] Ananthan, S., and Leishman, J. G., "Role of Filament Strain in the Free-Vortex Modeling of Rotor Wakes," *Journal of the American Helicopter Society*, Vol. 49, No. 2, Apr. 2004, pp. 176–191.

[43] Zhao, L., and Tsukamoto, H., "Hybrid Vortex Method for High Reynolds Number Flows Around Three-Dimensional Complex Boundary," *Computers and Fluids*, Vol. 36, No. 7, 2007, pp. 1213–1223.
doi:10.1016/j.compfluid.2007.01.003

[44] Pedersen, C. B., "An Indicial-Polhamus Model of Aerodynamics of Insectlike Flapping Wings in Hover," Ph.D. Thesis, Cranfield Univ. , Shrivenham, England, U.K., 17 June 2003.